Polar Cap Boundary identification using redline optical data and DMSP satellite particle data

B. Gallardo-Lacourt[1,2], S.Wing[3], L. Kepko[1], D. M. Gillies[4], E. L. Spanswick[4], E. A. Roy[4], E. F. Donovan[4]

[1]NASA Goddard Space Flight Center, Greenbelt, MD, USA
[2]Universities of Space Research Association, Columbia, MD, USA
[3]The Johns Hopkins University, Applied Physics Laboratory, Laurel, MD, USA
[4]Department of Physics & Astronomy, University of Calgary, Calgary, Alberta, Canada

Key Points:

- We compare the auroral poleward boundary determined using simultaneous optical and particle data during different geomagnetic conditions
- We find good agreement between the auroral boundary determined by auroral luminosity and those determined by particle flux
- Luminosity method can be applied during active geomagnetic conditions, providing high spatial and temporal resolution polar cap boundary

Corresponding author: B. Gallardo-Lacourt, bea.gallardolacourt@nasa.gov

Abstract

The location of the polar cap boundary is typically determined using low-orbit satellite measurements in which the boundary is identified by its unique signature of a sharp decrease in energy and particle flux poleward of the auroral oval. In principle, this decrease in precipitating particles should appear as a concomitant sharp change in auroral luminosity. Based on a few events, Blanchard et al. (1995) suggested that a dramatic gradient in redline aurora may also be an indicator of the polar cap boundary. In recent years, advances in capabilities and the deployment of ground-based all-sky imagers have ushered in a new era of auroral measurements. Auroral imaging has moved well beyond the capabilities of the instrumentation in the previous study in terms of both spatial and temporal resolution. We now have access to decades of optical data from arrays spanning a huge spatial range, enabling a fresh examination of the relationship between redline aurora, particle precipitation, and the polar cap open closed boundary. In this study, we use data from the DMSP satellites in conjunction with the University of Calgary's REGO (630.0nm) data to assess the viability of automated detection of the 2-dimensional polar cap boundary. Our results exhibit good agreement between the optical and particle polar cap boundary and suggest that a luminosity in redline emission could serve as a reasonable proxy for the location of the the electron poleward boundary during, while providing both high temporal and spatial resolution maps of the open-closed boundary.

Plain Language Summary

Named for its shape, the auroral oval is an oval-shaped region located near the north and south poles where the aurora is formed. Studying the location of the equatorward and poleward limits of the auroral oval is fundamental to evaluating the dynamics and responses of the near-Earth space environment. In particular, the poleward boundary corresponds to a region in which Earth's magnetic field transitions from closed (connected to Earth) to open field lines (connected to the solar wind); because of this topological change in magnetic field, the location of this boundary is fundamental to understand mass and energy transport in the whole magnetosphere-ionosphere system. While satellite data can determine the exact location of this boundary, they only provide point measurements. Auroral images are capable of detecting the luminosity around this boundary; however, many qualitative studies consider the region immediately poleward of this luminosity as the oval's poleward boundary. In this paper, we analyze the location of this boundary in a case study by using satellite data combined with auroral imaging data.

1 Introduction

The polar cap boundary corresponds to the region in which the Earth's magnetic field transitions from closed magnetic field lines connected to Earth, to open magnetic field lines that are connected to the solar wind. The location of the polar cap boundary reflects the amount of open magnetic flux in the polar cap. As the open magnetic flux increases or decreases, it can undergo poleward and equatorward motion in response to this change. This motion can be used as an indicator of the storage and release of magnetic energy within the magnetotail (Siscoe & Huang, 1985).

As described by Dungey (1961), when the solar wind Interplanetary Magnetic Field (IMF) has a southward component, reconnection takes place between the IMF and closed terrestrial field lines on the dayside magnetopause. This causes closed magnetospheric flux to become open to the solar wind. As one end of open magnetic field lines are connected to the solar wind flowing antisunward, they become swept into the magnetotail and represent stored magnetic energy. The accumulation of this open flux in the magnetosphere results directly in an increase of the area of the polar cap. This increase in polar cap size, produced by the ongoing dayside magnetic reconnection, is part of the substorm growth phase. Subsequently, the closure of open magnetic flux and release of stored magnetic energy through reconnection in the magnetotail that occurs during the substorm expansion phase causes a decrease in the polar cap area. Newly-closed field lines return to the dayside. Down-tail of the nightside reconnection site, field lines are once again reconnect and return to the IMF. The cycle of magnetic field lines from closed to open to closed again, which results from day-and nightside reconnection, is known as magnetospheric convection, or the Dungey cycle (e.g., Milan et al. (2003, 2021)).

In this cycle, reconnection rates are controlled by the IMF orientation upstream of the Earth on the dayside and by conditions in the magnetotail on the nightside. A knowledge, then, of temporal variations in polar cap area permits quantification of these reconnection rates that take place in regions that are currently difficult to monitor routinely with in situ observations. The reconnection-driven motion in the magnetosphere also imparts momentum to Earth's ionosophere. The magnetospheric convection cycle leads to ionospheric plasma drift in the two-cell convection pattern, with antisunward flow across the polar cap (open field lines) and return flow at lower latitudes (closed field lines). This ionospheric convection, when combined with a knowledge of the location of the polar cap boundary, can also be used to quantify the rate of reconnection.

Opposite to southward IMF conditions, when the IMF has a northward component "high-latitude reconnection" can take place with pre-existing open field lines in the magnetospheric lobes. Depending on whether individual solar wind magnetic field lines reconnect with both northern and southern lobes or reconnect with only one, it is thought that open magnetic flux can be closed or the amount of open flux in the system can remain unchanged, respectively (Cowley, 1981). In either case, a region of sunward ionospheric flow is predicted within the polar cap, and the dayside reconnection site no longer necessarily maps to the polar cap boundary.

Measurements of changes in polar cap area can therefore be utilized to help understand solar wind-magnetosphere coupling phenomena under both southward and northward IMF conditions. Previous studies have quantified changes in the magnetic flux around the polar cap boundary. For example, the expanding/contracting polar cap (ECPC) paradigm (e.g., Cowley and Lockwood (1992); Lockwood and Cowley (1992)) provides a quantitative method to examine the changes of magnetic flux—i.e., from open to closed field lines.

Previously, global imaging satellite provided a very useful tool to study the location of the polar cap boundary (Aikio et al., 2006), albeit with limited spatial resolution. Low orbit satellites carrying particle data detectors, such as DMSP and NOAA, provide a very precise determination of the location of the polar cap boundary, but along a single orbit

track, and limited to specific local times. Newell et al. (1996) developed an automatic algorithm to identify the location of different boundaries within and around the auroral oval using DMSP particle data. The polar rain electrons near the open-closed boundary on the nightside sometimes exhibit energy-latitude dispersion, in which the energy decreases with decreasing latitude (Wing & Zhang, 2015; Shirai et al., 1997). In addition, an early study by Blanchard et al. (1995) identified the location of the polar cap boundary by using redline imaging data and DMSP satellite. Moreover, several studies have found that there are sometimes discrepancies between the open-closed boundary identified by DMSP and those by optical data. However, the exact causes of these discrepancies are not entirely understood (e.g.,Boakes et al. (2008); Longden et al. (2010); Hubert et al. (2006)).

In this paper, we analyze the location of the polar cap boundary by taking advantage of the modern redline all-sky imagers (ASI), combined with DMSP satellites around the midnight sector. We compare DMSP particle boundaries to the red-line optical boundary. We also analyze if the location of the highest energy electrons in the dispersion region matches better the open-closed boundary identified in the optical data during moderate activity conditions.

The technological advancements of optical data in recent years allows us to perform this analysis with higher temporal and spatial resolution, potentially enabling routine, high temporal and spatial resolution maps of the 2-dimensional open-closed boundary.

2 Datasets and Methodology

We use data from the Defense Meteorological Satellite Program (DMSP) in conjunction with the University of Calgary's Redline Emission Geospace Observatory (REGO) all-sky imagers (ASI) to identify the polar cap boundary in particle and optical data respectively.

2.1 DMSP's electron and ion polar cap boundary identification

The Defense Meteorological Satellite Program (DMSP) is a Department of Defense program run by the Air Force Space and Missile Systems Center. Each DMSP satellite orbits the Earth in a sun-synchronous near-polar orbit with orbital period of ∼101 min at an altitude of ∼835 km above the surface of the Earth. The DMSP satellites carry the Special Sensor J (SSJ) instrumental package that uses curved plate electrostatic analyzers to measure ion and electron at energies between 30 eV to 30 keV in 19 logarithmically equally spaced steps at 1s temporal resolution (Hardy, 1984). DMSP satellites are used here to determine the electron and ion polar cap boundary.

We use the particle flux measurements from the DMSP 16 and 18 satellites to identify the auroral oval's poleward boundary. Newell et al. (1996) developed an automated algorithm to identify auroral electron and ion poleward boundaries, the b5e and b5i, respectively, where the precipitating electron and ion differential energy flux drop off sharply, typically by an order of magnitude over a short distance ($< 0.2°$). Usually, the b5e and b5i are close to each other in latitude. In addition, Newell et al. (1996) defined the b6 boundary as the poleward edge of the subvisual drizzle, which is the region of weak ion and electron precipitation. Typically, b6 is located poleward of both b5e and b5i. Previous studies used b6 or b5e(for electrons) or b5i (for ions) as a demarcation of the open-closed boundary (e.g., Newell et al. (1996), Boakes et al. (2008), Longden et al. (2010)). The present study uses b5e and b5i as a starting point for the open-closed boundary, but these boundaries are further inspected manually and modified as described next.

The Newell et al. (1996) boundary identification algorithm was developed to give a measure of the poleward-most location of ion and electron precipitation that originate from the plasma sheet. This algorithm works well in general and can be very useful for statistical studies where it would be prohibitively too laborious to check manually. However, for case

studies, it is prudent to inspect the boundaries manually because, as with most automated algorithm, the poleward boundary identification algorithm is not perfect, and sometimes fails to identify the boundary. Hence, in order to get the most accurate locations of ion and electron open-closed boundaries, we visually identify separate open-closed boundaries for ions and electrons. The open-closed boundary for ion precipitation is the location of the poleward most ions that originate from the plasma sheet (ions having the characteristics of plasma sheet ions (Wing & Newell, 1998, 2002; Wing et al., 2005). The same definition is used to determine the electron open-closed boundary. Sometimes, they coincide with the b5e and b5i,respectively, but other times they do not. In cases where they do not, we use the boundaries that are determined manually as they are deemed to be more accurate.

2.2 Redline Emission Geospace Observatory (REGO) luminosity at the polar cap boundary

In Earth's upper atmosphere, auroral red-line (630.0 nm) emission is produced by the transition of atomic oxygen from an excited state to the ground state (Link & Cogger, 1988; Solomon et al., 1988; Gillies et al., 2017). The REGO array is composed of nine all-sky cameras covering a large portion of the North American sector. Each camera operates at a high temporal resolution of 3-s cadence and 2-s exposure time. REGO is sensitive to wavelengths between ∼628 and 632 nm, with a maximum at 630.0 nm (Liang et al., 2016). As a manifestation of its sensitivity, the REGO imagers located at poleward latitudes can easily detect faint polar cap patches—which are often no more than several tens of Rayleigh in intensity—and their subtle spatial/temporal variations (e.g., Zou et al. (2015)). This characteristic is particularly important for this study, in which we analyze the luminosity within the polar cap in order to identify a proxy for the auroral oval's poleward boundary.

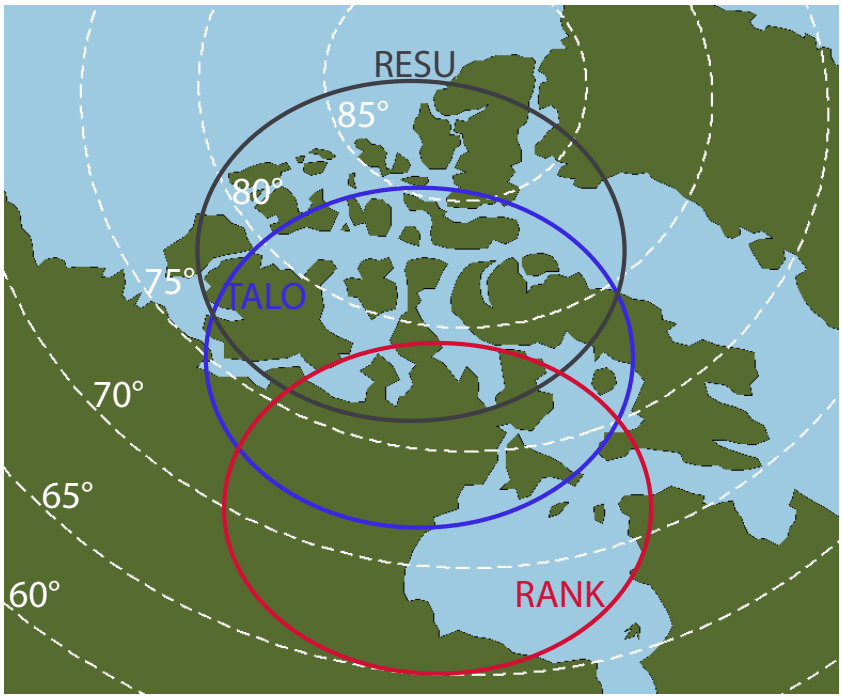

Figure 1. Coverage of the REGO imagers used in this analysis. From north to south the cameras are located at Resolute Bay (RESU) in dark blue, Taloyoak (TALO) in blue, and Rankin Inlet (RANK) in red.

All-sky imagers (ASIs) provide luminosity as counts that corresponds to the number of photons per unit area or pixel. To compare luminosities between different cameras, we convert these arbitrary units (count) to Rayleigh (R). The calibration procedure takes into consideration the minimum luminosity that REGO's charge-couple device (CCD) detector is able to register, the so-called dark frame correction. In addition, flat field and the Van Rhijn corrections are applied (Van Rhijn, 1924; Roach & Meinel, 1965). Finally, Rayleigh conversion parameters are introduced using calibration parameters established in the in-house calibration performed prior to the instruments' deployment by the University of Calgary. The ASIs used in our analysis are located at Resolute Bay (RESU), Taloyoak (TALO), and Rankin inlet (RANK), and their coverage is represented in Figure 1.

2.3 Analysis approach

We analyzed events when DMSP satellites crossed the polar cap boundary within the FOV of Rankin Inlet (RANK) ASI and Taloyoak (TALO). The best relationship between the observed polar cap boundary and nightside reconnection would occur near local midnight, where field lines map the the nightside plasmasheet. Yet, for the period of 2014-2016 that we examined for this study, the available DMSP satellites are more dawn-dusk. DMSP-16 and 18 provided reasonable coverage with the poleward cameras at Rankin Inlet (RANK) and Taloyoak (TALO) during early and late morning hours.

To quantify the background luminosity at the time the satellite crosses the electron poleward boundary, we have used the ASI poleward of RANK and TALO at Resolute Bay (RESU), which lies in the polar cap. The events selected for this study occurred in the absence of polar cap structures such as polar cap patches or polar cap arcs, and allowed us to identify the luminosity levels in absence of precipitation or optical structures within the polar cap. We have analyzed the minimum luminosity within RESU at the center of the polar cap during one hour, $\pm$ 30 minutes around the time when DMSP satellite crosses the electron poleward boundary. One of the advantages of RESU ASI is that is well within the polar cap (above 80 degrees magnetic latitude), and it rarely captures the luminosity from the auroral oval. For this analysis we have used RESU as the primary ASI to calculate the luminosity within the polar cap and discarded potential events in which structures (e.g., polar cap patches and arcs) were observed in this region as previously described.This luminosity is then compared to the luminosity along the DMSP orbit within REGO or TALO. Finally, for the comparison we have calculated the luminosity poleward of the electron boundary within RANK. Figure 1b shows the region from which the polar cap luminosity is obtained and a mean value is obtained for the analysis. In the following case study we present similar plots to analyze the polar cap luminosity.

3 Results

For all case studies presented below, in-situ particle data were analyzed from DMSP-16 and DMSP-18 for events in which the satellites crossed close to the center of the ASI field-of-view (FOV). The camera at Rankin Inlet (RANK) was used for five out of the six events analyzed here; Taloyoak(TALO) was used for the sixth. All the case study events occurred between 2014 and 2016. Figure 2 shows the AL indices for each event, with a vertical line marking the time at which DMSP crossed the electron poleward boundary. Events 1 and 4 occurred approximately 90 minutes after a substorm onset, during the recovery phase of a substorm. Events 2 and 6 took place during the expansion phase, while event 5 occurred $\sim$ 40 minutes before an AL decrease of $\sim$200 nT. Finally, event 3 occurred during quiet time with an AL index of $\sim$ -20 nT. In the following subsections, we discuss these six representative events in detail.

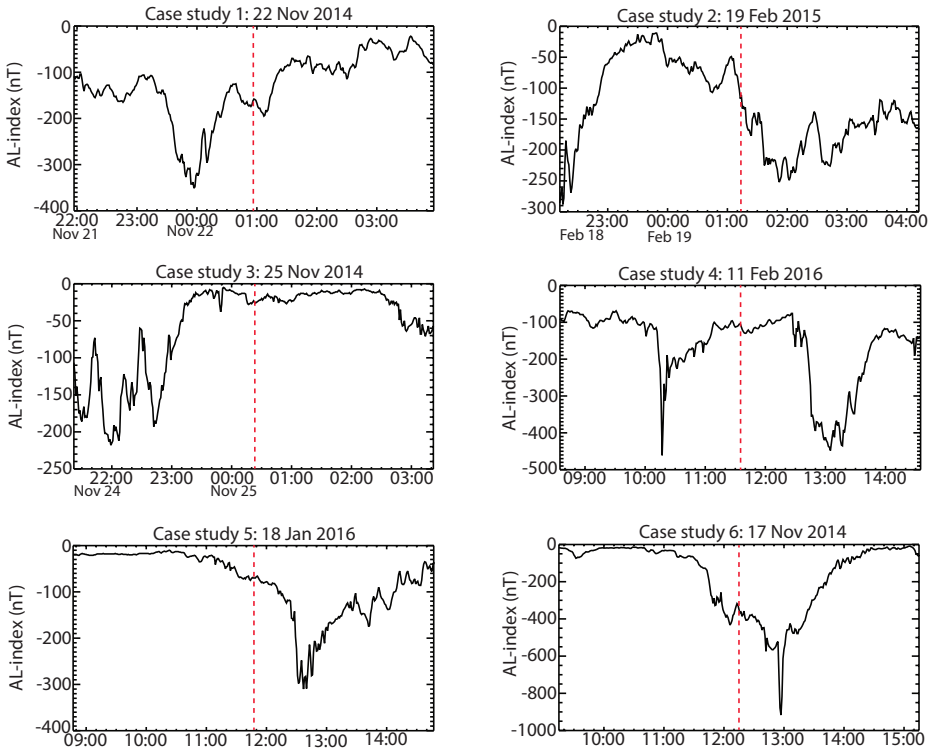

Figure 2. AL indices for all the events. The red vertical line indicates the time at which the DMSP satellites crosses the electron poleward boundary.

3.1 Case study one: 22 November 2014

On 22 November 2014, the DMSP-18 satellite crossed close to the center of the FOV of the REGO ASI at RANK. We extracted the luminosity along the satellite track and then compared it with particle data from the DMSP-18 satellite. To calculate the luminosity along the satellite track over RANK, we computed the nearest location to the satellite within the ASI via the nearest-neighbor mathematical approach. This procedure was performed every three seconds, corresponding to the imager's temporal resolution. This produced a time-series at 3-s resolution of auroral luminosity along the spacecraft's ground track while within the FOV of RANK. To reduce variability due to image noise, we calculated an average luminosity at that location by obtaining the mean over an area of five by five pixels. This luminosity was then contrasted with those obtained poleward of the electron and ion boundary within the same ASI, and it was also compared with an ASI located poleward, well within the polar cap.

Figure 3a shows the increased luminosity within the auroral oval detected at RANK at 11:47:27 UT, which corresponds to the time when DMSP-18 crossed the electron poleward boundary. The orbit of DMSP satellite is indicated by the green line within the image. The red and blue circles correspond to the location of the DMSP electron and ion poleward boundary, respectively, along the satellite's orbit. The white-dashed contour line corresponds to 75° magnetic latitude (mlat). For all the events analyzed, the ASI data and DMSP satellite's orbit have been mapped to the redline nominal emission height of 230 km (Solomon et al., 1988; Gillies et al., 2017).

Figure 3b shows the polar cap at RESU. From top to bottom, the white dashed contour lines correspond to 85°, 80°, and 75° magnetic latitude, respectively. We calculated the

luminosity within the polar cap at the center of the RESU FOV, in the area highlighted by the yellow quadrilateral. The polar cap luminosity is equal to the mean value inside the highlighted area during a time interval of ±30 minutes centered on the time when DMSP-18 crossed the electron poleward boundary. During this period, we did not detect any optical structure within the polar cap (e.g., polar cap patches and arcs).

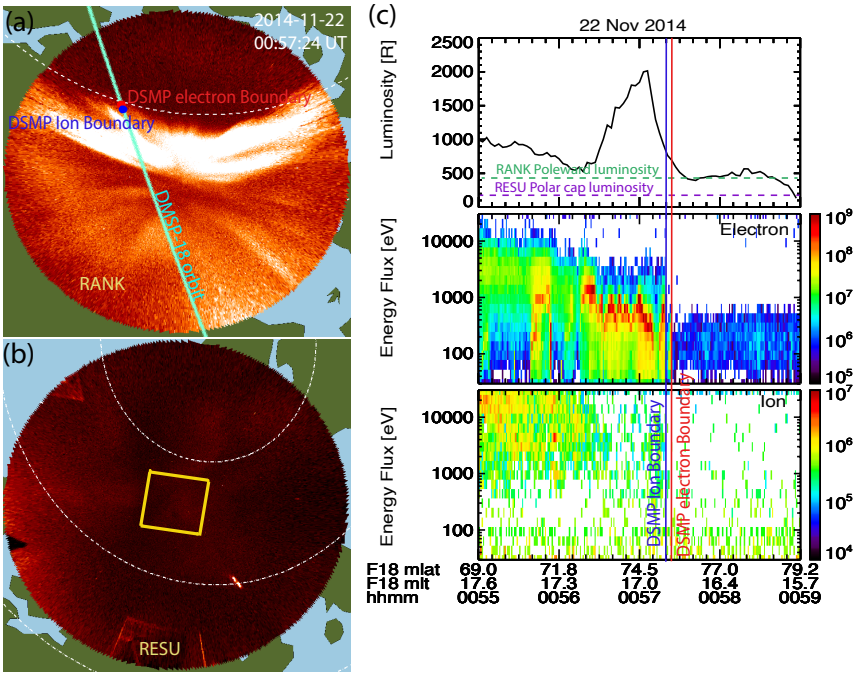

Figure 3. Case study one on 22 November 2014. (a) REGO ASI at Rankin Inlet (RANK) detected the polar cap boundary location while DMSP-18 satellite crossed closer to the ASI FOV (green line). The red (blue) circle indicates the location of the electron (ion) poleward boundary along the satellite track. (b) Luminosity within Resolute bay (RESU), located poleward of RANK and measuring the polar cap. (c) From top to bottom the panels represents the luminosity along DMSP-18 satellite track, electron and ion energy flux.

Particle data from the DMSP Special Sensor for Precipitating Particles (SSJ4) detector were obtained along the DMSP-18 orbit and can be observed in Figure 1c. From top to bottom the panels represent the luminosity extracted from RANK along the satellite track every three seconds, and the electron and the ion energy flux from DMSP-18 satellite. The green and purple horizontal lines correspond to the luminosity detected poleward of the electron and ion DMSP baundaries at RANK, and the luminosity within the polar cap obtained at RESU, respectively. As the satellite progressed poleward, it crossed through plasmasheet field lines, as indicated by the electron precipitation extending from below 69° mlat to ∼ 75° mlat and the ion precipitation spanning a similar region. The DMSP electron and ion boundaries are shown with vertical red and blue lines. Note that the ion energy flux decreases at about 73° mlat, equatorward of the sharp electron flux decrease. However, there is still weak precipitation equatorward of ∼ 75° that is distinct from the nearly absent flux in the polar cap.

The luminosity along the satellite orbit, shown in the first panel of Figure 3c, exhibits a broad increase in luminosity equatorward of the DMSP boundaries corresponding to the arc visible in Figure 3a. The RANK poleward luminosity decreases abruptly near the

DMSP electron boundaries, and intercepts the luminosity curve $\sim 0.3°$ mlat poleward of the DMSP poleward boundary. Similarly, the maximum luminosity, a feature commonly used to qualitatively identify the poleward boundary, is located $\sim 0.6°$ mlat equatorward of the true electron poleward boundary.

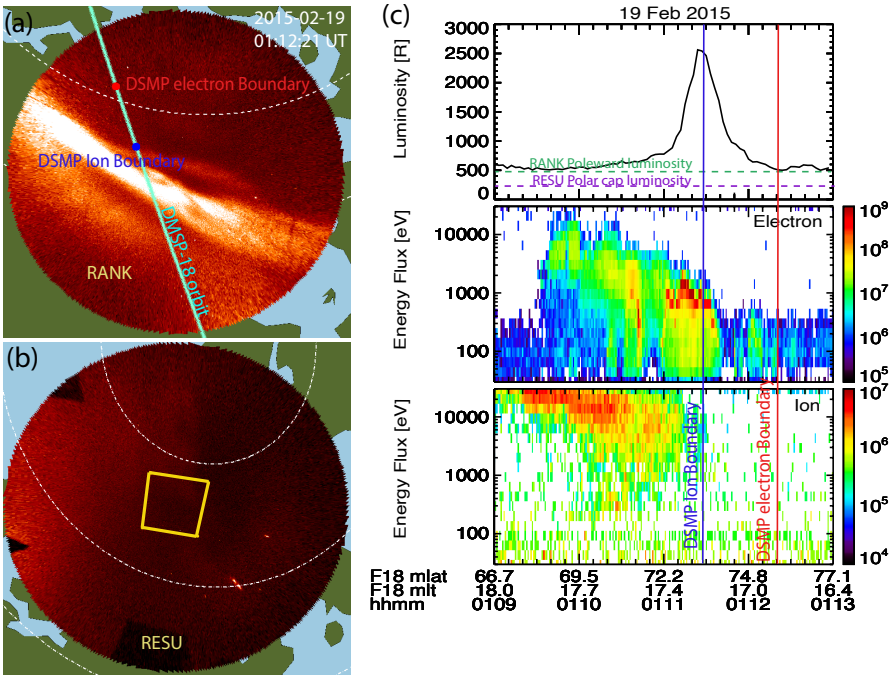

Figure 4. Case study two on 19 February 2015 at RANK. The figure format is the same as in Figure 1.

3.2 Case study two: 19 February 2015

Figure 4 shows our second event, from 19 February 2015, in the same format as Figure 3. REGO at RANK (Figure 4a) observed a broad region of diffuse emission equatorward of a bright arc, while RESU, just poleward of RANK, observed no auroral emission (Figure 4b). DMSP-18 traveled the region from low to high latitudes crossing very near the center of the RANK FOV. In Figure 4a, the red and blue circles represent DMSP's electron and ion poleward boundary location along the satellite orbit, respectively. Figure 2c shows from top to bottom the luminosity along DMSP-18 satellite orbit, the electron flux, and the ion flux. For this event, as observed in Figures 4a and 4c, the ion boundary is located several degrees ($\sim 2°$ mlat) equatorward than the electron poleward boundary. While the ion poleward boundary lies closer to the maximum luminosity (Figure 2c), the electron boundary is located several degrees poleward.

The horizontal lines in the upper panel in Figure 2c corresponds to the luminosity recorded poleward from the electron and ion boundaries at RANK (green) and RESU (purple). Similar to the first event, the luminosity detected poleward within RANK provides a good reference for the location of electron poleward boundary demarcated by the green horizontal lines intercepting the luminosity along the satellite's orbit at the same location as the DMSP's electron poleward boundary. For this event, the maximum luminosity within the auroral oval is roughly collocated with the ion poleward boundary (blue vertical line).

3.3 Case study three: 25 November 2014

The third case study and the last event in conjunction with the DMSP-18 satellite took place on November 25, 2014. During this event the auroral oval extended poleward of 75° mlat covering most of the RANK FOV; however, the poleward camera at TALO was able to record the location of the boundary. Figure 3a shows the optical poleward boundary at TALO and the DMSP-18 orbit. The red and blue circles corresponds to the DMSP electron and ion boundary respectively, detected along the satellite's orbit. Figure 5b shows the luminosity within the polar cap at RESU. The diffuse high-luminosity area in the lower-right sector of RANK and lower-left area of RESU is moon contamination.

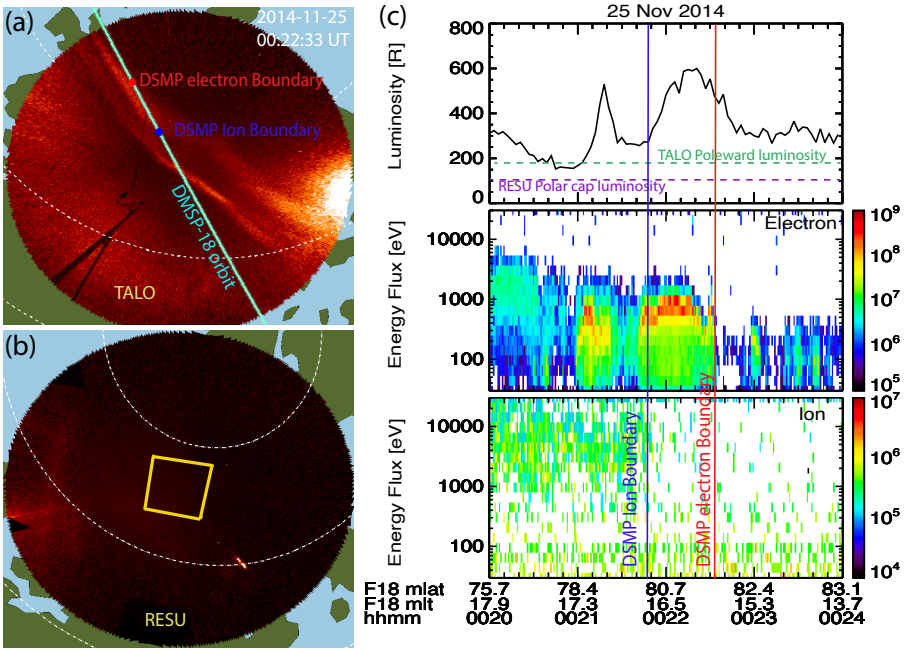

Figure 5. Case study three occurred on November 25, 2014. During this event, the auroral oval extended poleward of RANK and the analysis was done with TALO. The green line corresponds to the DMSP-18 orbit crossing TALO FOV and the red (blue) circle are the electron (ion) boundary along the satellite's track. Figure 5b and c have the same format as in Figure 1b and c respectively.

Figure 5c shows from top to bottom the luminosity from TALO along DMSP-18 satellite orbit, the electron energy flux, and the ion energy flux. For this event, DMSP-18 traveled poleward crossing the electron poleward boundary at ∼00:22:33 UT. DMSP-18 crossed first the ion poleward boundary at ∼00:21:50 UT (blue vertical line) and the electron poleward boundary after 00:22:30 (red vertical line). For this event, the electron poleward boundary was located ∼ 2° poleward than the ion bounday. We used the two poleward luminosities, at TALO and RESU (green and purple horizontal lines respectively), to estimate the location the electron boundary from the optical data. At the time of the satellite crossing, the ion poleward boundary was located more than one degree equatorward than the electron poleward boundary. The two main regions of electron precipitation (Figure 5c middle panel) can be easily visualized as the two regions of enhanced luminosity along the satellite track (Figure 5, first panel). Although the luminosity starts decreasing following the electron precipitation population, the luminosity at TALO does not reach either the TALO or RESU poleward luminosities, indicated by horizontal lines. This is likely due to the satellite footprint skimming the most poleward arc, as observed in Figure 5a.

3.4 Case study four: 11 February 2016

The fourth case study occurred on 11 February 2016. Figure 6a shows the satellite orbit overlaid on REGO at RANK. During this event, the satellite traveled from high to low latitudes, crossing first the ion poleward boundary and then the electron boundary at 11:35:54 UT.. The polar cap luminosity was calculated at the center of the REGO at RESU, highlighted by the yellow rectangle in Figure 6b. In addition, the poleward luminosity was extracted from REGO at RANK by selecting the region poleward of the electron boundary. These calculation have been used as the poleward luminosity in the first panel of Figure 6c, shown with horizontal dashed lines. From top to bottom, Figure 6c shows the luminosity along DMSP-16 satellite track, with the red and blue vertical lines representing the electron and ion poleward boundary respectively. The ion boundary was located a fraction of a degree poleward of the electron boundary. Both of the poleward luminosities, at RESU and RANK, are reasonable proxies for the electron and ion boundaries in this event, with the intersection between the electron poleward boundary (red vertical line) and the poleward luminosity measured at RANK (dashed-green horizontal line) occurring near the time when the luminosity along the orbit starts increasing.

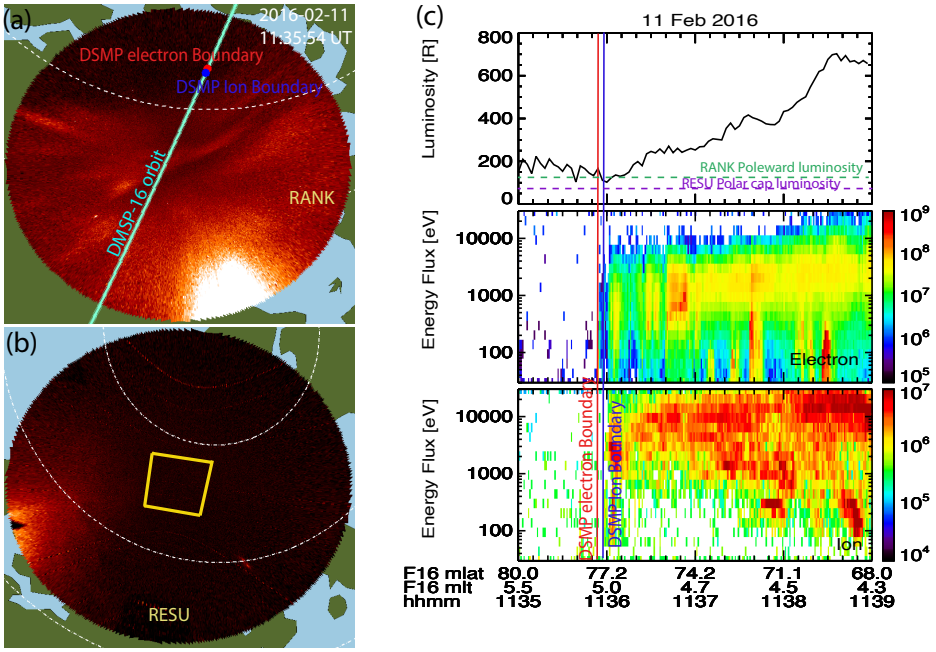

Figure 6. Case study fourth occurred on February 11, 2016. (a) During this event, DMSP -16 satellite crossed the poleward boundary within the RANK FOV. (b) Luminosity observed poleward of RANK at RESU. (c) From top to bottom: Luminosity along DMSp-16 satellite, electron energy flux, and ion energy flux. The green and purple lines correspond to the the poleward luminosty at RANK and RESU, respectively. The red (blue) circle are the electron (ion) boundary along the satellite's track.

3.5 Case study five: 18 January 2016

On 18 January 2016 DMSP-16 crossed the poleward boundary within the FOV of REGO-RANK. Figure 7a shows the orbit of DMSP-16 across the RANK camera's FOV. The red and blue circles in Figure 7a indicates the location at which the satellite crosses the electron and ion poleward boundary respectively. During this event, the electron poleward

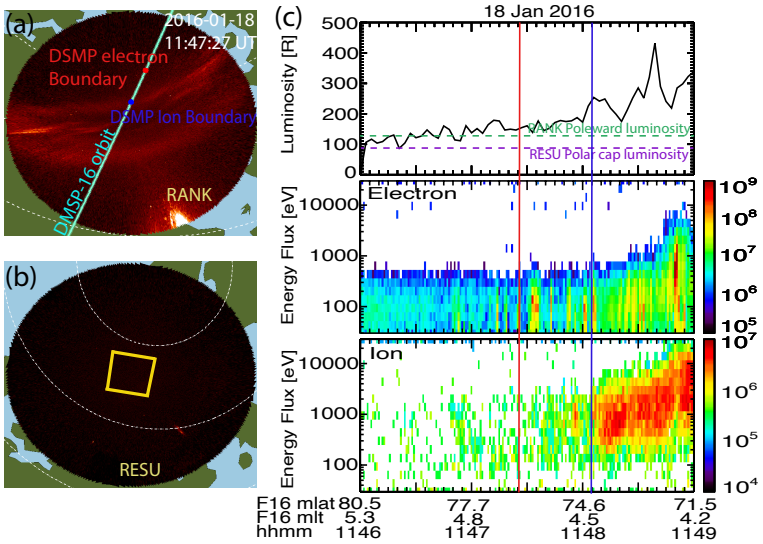

Figure 7. Case study five shows the DMSP-16 satellite transit above RANK all-sky imager (ASI) on 18 January 2016. THE ASI at RESU is located poleward than RANK and it has been used to identified luminosity levels within the polar cap region. The figure format is the same as in Figure 1.

boundary was located couple of degrees poleward from the ion boundary. The polar cap luminosity and particle boundaries were obtained in the same manner as described for the previous events. As shown in 7c, the ion boundary (blue vertical line) is located equatorward of the electron boundary (red vertical line). The luminosity along the track of DMSP intercepts the polar cap luminosity closer to the location of the electron boundary, making the poleward luminosity at RANK a good proxy to determine the location of the electron poleward boundary. Similar to previous events, the polar cap luminosity detected at RESU is $\sim$ 200 [R] dimmer than the RANK poleward luminosity.

3.6 Case study six: 17 November 2014

On 17 November 2014, DMSP-16 crossed the poleward boundary at REGO-RANK. Figure 8a shows the orbit of DMSP-16 across the RANK camera's FOV. The red and blue circles in Figure 8a indicates the location at which the satellite crosses the electron and ion poleward boundary respectively. During this event, both poleward particle boundaries were closely located, with the ion boundary located slightly poleward of the electron boundary. The luminosity along the DMSP orbit track intercepts the RANK poleward luminosity at the location of the electron particle boundary. Similar to previous events, the polar cap luminosity detected at RESU is $\sim$ 200 [R] dimmer than the RANK poleward luminosity.

4 Discussion and Conclusions

In this paper, we calculated the location of the polar cap boundary with 2 independent methods by taking advantage of conjunctions between high temporal and spatial resolution redline imagers and DMSP satellites. Our analysis has enabled us to obtain a good optical proxy for the location of the DMSP polar cap boundary. We analyzed the luminosity poleward from the DMSP boundary from two ASIs. Our findings suggests that the luminosity poleward from the same camera could be used to estimate the location of the polar cap boundary. In addition, the luminosity obtained from a different camera located well

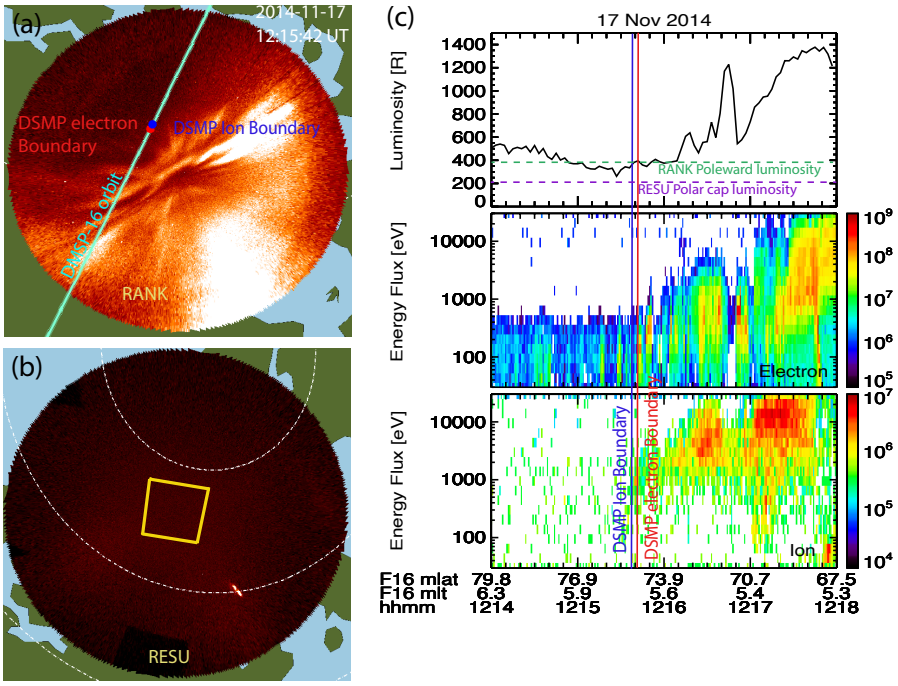

Figure 8. Case study six shows the conjunction between RESU at RANK and DMSP-16 satellite on 17 November 2014 at RANK. The figure format is the same as in Figure 1.

within the polar cap demonstrated that these luminosities were too low compared to the real location of the polar cap boundary. A possible explanation for this discrepancy could be associated with the scattered light of the aurora within the FOV of the camera, making the background levels slightly higher than they would be without bright aurora.

As demonstrated in this analysis, the REGO ASI array provides high temporal and spatial resolution observations of the auroral oval. A combination of the REGO capabilities and the method developed in this paper, allows us to derive the location of the polar cap boundary with high temporal and spatial resolution. To demonstrate the potential of our methodology, we have calculated the derived location of the polar cap boundary for the 2-dimensional REGO data during the first case study, 22 November 2014. As established previously, we have compared the luminosity poleward of the DMSP electron polar cap boundary within the same ASI, with that detected at constant longitudinal cuts along the image. Figure 9 shows the results of applying our methodology to define the 2-dimensional polar cap boundary (yellow line) at three different times around case study 1. By comparing these luminosities, in the same way we did for the case studies, along the DMSP satellites orbit, we were able to obtain the derived location of the poleward boundary at different locations and times.

We calculated the location of the polar cap boundary using two different datasets by taking advantage of conjunctions between high temporal and spatial resolution redline imagers and DMSP satellites. Our analysis has shown that the luminosity within the poleward region of the same ASI could be used as an indicator for the location of the electron poleward boundary location. In particular, the poleward luminosity calculated within the same ASI where the satellite crosses the boundaries appear to intercept the luminosity along the satellite track closest to the electron equatorward boundary location.

We have also analyzed the AL indices for the six events examined in this case study. We found that the six events occur during different geomagnetic conditions showing that some events occurred at differed substorm stages and some during quiet time. Although the conditions during these events are significantly different, the method explored here to identify the polar cap boundary location by using the luminosity poleward of the boundaries, has proven successful independent of the geomagnetic conditions. However, some open questions remain regarding the use of this method to identify the boundary during a substorm evolution. During the substorm evolution–growth, onset, expansion, and recovery phases–the auroral oval expands and contract, sometimes very rapidly. A future analysis and a great test of the method presented here, is to study the applicability of this analysis continuously during the evolution of different substorms.

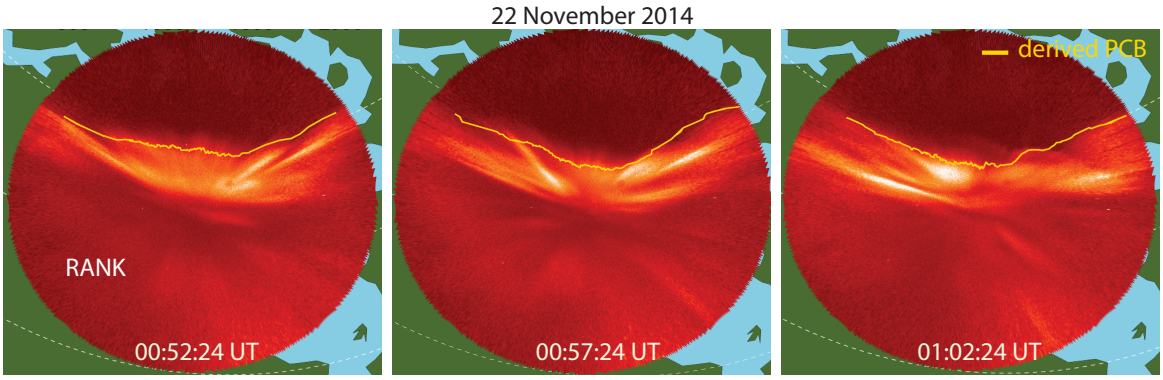

Figure 9. Derived polar cap boundary from the methodology developed in the paper. The yellow line corresponds to the polar cap boundary derived by using the poleward luminosity from RANK ASI at three different times.

Acknowledgments

The Redline Auroral Geospace Observatory (REGO) is a joint Canada Foundation for Innovation and Canadian Space Agency project developed by the University of Calgary. The REGO data is available from the University of Calgary data website at `https://data.phys.ucalgary.ca/`. The calibration documentation and procedures can be obtained from the University of Calgary's data web-page. DMSP's SSJ particle data can be obtained from the JHU/APL website at `http://sd-www.jhuapl.edu/Aurora/data/data_step1.cgi` . BGL was supported by a NASA Postdoctoral Program (NPP) fellowship. SW acknowledges the support of NASA grants 80NSSC20K0704 and NNZ16AQ87G. LK was supported by the NASA competed internal scientist funding model (ISFM).

References

Aikio, A. T., Pitkänen, T., Kozlovsky, A., & Amm, O. (2006). Method to locate the polar cap boundary in the nightside ionosphere and application to a substorm event. *Annales Geophysicae*, *24*(7), 1905–1917. Retrieved from `https://angeo.copernicus.org/articles/24/1905/2006/` doi: 10.5194/angeo-24-1905-2006

Blanchard, G. T., Lyons, L. R., Samson, J. C., & Rich, F. J. (1995). Locating the polar cap boundary from observations of 6300 Å auroral emission. *Journal of Geophysical Research: Space Physics*, *100*(A5), 7855-7862. Retrieved from `https://agupubs.onlinelibrary.wiley.com/doi/abs/10.1029/94JA02631` doi: https://doi.org/10.1029/94JA02631

Boakes, P. D., Milan, S. E., Abel, G. A., Freeman, M. P., Chisham, G., Hubert, B., & Sotirelis, T. (2008). On the use of image fuv for estimating the latitude of the open/closed magnetic field line boundary in the ionosphere. *Annales Geophysicae*, *26*(9), 2759–2769. Retrieved from https://angeo.copernicus.org/articles/26/2759/2008/ doi: 10.5194/angeo-26-2759-2008

Cowley, S. (1981). Magnetospheric asymmetries associated with the y-component of the imf. *Planetary and Space Science*, *29*(1), 79-96. Retrieved from https://www.sciencedirect.com/science/article/pii/0032063381901410 doi: https://doi.org/10.1016/0032-0633(81)90141-0

Cowley, S., & Lockwood, M. (1992). Excitation and decay of solar-wind driven flows in the magnetosphere-ionosphere system. *Annales Geophysicae*, *10*, 103-115.

Dungey, J. W. (1961). Interplanetary Magnetic Field and the Auroral Zones. *Physical Review Letters*, *6*(2), 47. Retrieved from http://adsabs.harvard.edu/cgi-bin/nph-data_query?bibcode=1961PhRvL...6...47D\&link_type=EJOURNAL doi: 10.1103/physrevlett.6.47

Gillies, D. M., Knudsen, D., Donovan, E., Jackel, B., Gillies, R., & Spanswick, E. (2017). Identifying the 630 nm auroral arc emission height: A comparison of the triangulation, fac profile, and electron density methods. *Journal of Geophysical Research: Space Physics*, *122*(8), 8181-8197. Retrieved from https://agupubs.onlinelibrary.wiley.com/doi/abs/10.1002/2016JA023758 doi: https://doi.org/10.1002/2016JA023758

Hardy, D. (1984). Precipitating electron and ion detectors (ssj/4) for the block 5d/flights 6-10 dmsp (defense meteorological satellite program) satellites: Calibration and data presentation. *Rep. AFGL-TR-79-0216, Air Force Geophys. Lab., Hanscom Air Force Base, Mass*.

Hubert, B., Milan, S. E., Grocott, A., Blockx, C., Cowley, S. W. H., & Gérard, J.-C. (2006). Dayside and nightside reconnection rates inferred from image fuv and super dual auroral radar network data. *Journal of Geophysical Research: Space Physics*, *111*(A3). Retrieved from https://agupubs.onlinelibrary.wiley.com/doi/abs/10.1029/2005JA011140 doi: https://doi.org/10.1029/2005JA011140

Liang, J., Donovan, E., Jackel, B., Spanswick, E., & Gillies, M. (2016). On the 630 nm red-line pulsating aurora: Red-line emission geospace observatory observations and model simulations. *Journal of Geophysical Research: Space Physics*, *121*(8), 7988-8012. Retrieved from https://agupubs.onlinelibrary.wiley.com/doi/abs/10.1002/2016JA022901 doi: https://doi.org/10.1002/2016JA022901

Link, R., & Cogger, L. L. (1988). A reexamination of the o i 6300-Å nightglow. *Journal of Geophysical Research: Space Physics*, *93*(A9), 9883-9892. Retrieved from https://agupubs.onlinelibrary.wiley.com/doi/abs/10.1029/JA093iA09p09883 doi: https://doi.org/10.1029/JA093iA09p09883

Lockwood, M., & Cowley, S. (1992). Ionospheric convection and the substorm cycle. In *the first international conference on substorms, ics-1* (pp. 99–109). Retrieved from http://centaur.reading.ac.uk/38835/

Longden, N., Chisham, G., Freeman, M. P., Abel, G. A., & Sotirelis, T. (2010). Estimating the location of the open-closed magnetic field line boundary from auroral images. *Annales Geophysicae*, *28*(9), 1659–1678. Retrieved from https://angeo.copernicus.org/articles/28/1659/2010/ doi: 10.5194/angeo-28-1659-2010

Milan, S. E., Carter, J. A., Sangha, H., Bower, G. E., & Anderson, B. J. (2021). Magnetospheric flux throughput in the dungey cycle: Identification of convection state during 2010. *Journal of Geophysical Research: Space Physics*, *126*(2), e2020JA028437. Retrieved from https://agupubs.onlinelibrary.wiley.com/doi/abs/10.1029/2020JA028437 (e2020JA028437 2020JA028437) doi: https://doi.org/10.1029/2020JA028437

Milan, S. E., Lester, M., Cowley, S. W. H., Oksavik, K., Brittnacher, M., Greenwald, R. A., ... Villain, J.-P. (2003). Variations in the polar cap area during two substorm cycles. *Annales Geophysicae*, *21*(5), 1121–1140. Retrieved from https://angeo.copernicus

.org/articles/21/1121/2003/ doi: 10.5194/angeo-21-1121-2003

Newell, P. T., Feldstein, Y. I., Galperin, Y. I., & Meng, C.-I. (1996). Morphology of nightside precipitation. *Journal of Geophysical Research: Space Physics*, *101*(A5), 10737-10748. Retrieved from https://agupubs.onlinelibrary.wiley.com/doi/abs/10.1029/95JA03516 doi: https://doi.org/10.1029/95JA03516

Roach, F. E., & Meinel, A. B. (1965). The height of the nightglow by the van rhijn method. *Astrophysical Journal*, *122*, 530-553.

Shirai, H., Maezawa, K., Fujimoto, M., Mukai, T., Yamamoto, T., Saito, Y., ... Kaya, N. (1997). Drop-off of the polar rain flux near the plasma sheet boundary. *Journal of Geophysical Research: Space Physics*, *102*(A2), 2271-2278. Retrieved from https://agupubs.onlinelibrary.wiley.com/doi/abs/10.1029/96JA02600 doi: https://doi.org/10.1029/96JA02600

Siscoe, G. L., & Huang, T. S. (1985). Polar cap inflation and deflation. *Journal of Geophysical Research: Space Physics*, *90*(A1), 543-547. Retrieved from https://agupubs.onlinelibrary.wiley.com/doi/abs/10.1029/JA090iA01p00543 doi: https://doi.org/10.1029/JA090iA01p00543

Solomon, S. C., Hays, P. B., & Abreu, V. J. (1988). The auroral 6300 Å emission: Observations and modeling. *Journal of Geophysical Research: Space Physics*, *93*(A9), 9867-9882. Retrieved from https://agupubs.onlinelibrary.wiley.com/doi/abs/10.1029/JA093iA09p09867 doi: https://doi.org/10.1029/JA093iA09p09867

Van Rhijn, P. J. (1924). *Bulletin of the astronomical institutes of the Netherlands*, *2*(75). doi: 10.1086/146115

Wing, S., Johnson, J. R., Newell, P. T., & Meng, C.-I. (2005). Dawn-dusk asymmetries, ion spectra, and sources in the northward interplanetary magnetic field plasma sheet. *Journal of Geophysical Research: Space Physics*, *110*(A8). Retrieved from https://agupubs.onlinelibrary.wiley.com/doi/abs/10.1029/2005JA011086 doi: https://doi.org/10.1029/2005JA011086

Wing, S., & Newell, P. T. (1998). Central plasma sheet ion properties as inferred from ionospheric observations. *Journal of Geophysical Research: Space Physics*, *103*(A4), 6785-6800. Retrieved from https://agupubs.onlinelibrary.wiley.com/doi/abs/10.1029/97JA02994 doi: https://doi.org/10.1029/97JA02994

Wing, S., & Newell, P. T. (2002). 2d plasma sheet ion density and temperature profiles for northward and southward imf. *Geophysical Research Letters*, *29*(9), 21-1-21-4. Retrieved from https://agupubs.onlinelibrary.wiley.com/doi/abs/10.1029/2001GL013950 doi: https://doi.org/10.1029/2001GL013950

Wing, S., & Zhang, Y. L. (2015). The nightside magnetic field line open–closed boundary and polar rain electron energy-latitude dispersion. *Annales Geophysicae*, *33*(1), 39–46. Retrieved from https://angeo.copernicus.org/articles/33/39/2015/ doi: 10.5194/angeo-33-39-2015

Zou, Y., Nishimura, Y., Lyons, L. R., Shiokawa, K., Donovan, E. F., Ruohoniemi, J. M., ... Nishitani, N. (2015). Localized polar cap flow enhancement tracing using airglow patches: Statistical properties, imf dependence, and contribution to polar cap convection. *Journal of Geophysical Research: Space Physics*, *120*(5), 4064-4078. Retrieved from https://agupubs.onlinelibrary.wiley.com/doi/abs/10.1002/2014JA020946 doi: https://doi.org/10.1002/2014JA020946